ICAS PAPER No. 72 – 20

THE DEVELOPMENT OF INLET FLOW DISTORTIONS IN MULTI-STAGE AXIAL COMPRESSORS OF HIGH HUB-TIP RATIO

by
Hans Mokelke, Research Student
S. R. C. Turbomachinery Laboratory
Cambridge University, U. K.

The Eighth Congress of the International Council of the Aeronautical Sciences

INTERNATIONAAL CONGRESCENTRUM RAI-AMSTERDAM, THE NETHERLANDS
AUGUST 28 TO SEPTEMBER 2, 1972

Price: 3. Dfl.

THE DEVELOPMENT OF INLET FLOW DISTORTIONS IN MULTI-STAGE AXIAL COMPRESSORS OF HIGH HUB-TIP RATIO

H. Mokelke
S.R.C. Turbomachinery Laboratory
Cambridge University Engineering Department
Cambridge, England

Abstract

A small perturbation theory is presented for the prediction of circumferential flow distortions in high hub-tip ratio multi-stage axial compressors with inlet maldistribution. The analytical model replaces the stages by actuator discs. Numerical examples have been presented which demonstrate the influence of varying stage characteristics on the attenuation of the distortions and which show how the distorted flow redistributes in large axial clearances within a compressor. The theory has been compared with interstage traverse data obtained from a 4-stage axial flow compressor. Results show that circumferential crossflow within the compressor is small but further numerical evidence indicates that crossflow may become significant as the number of stages, and hence the overall gap length, increase.

I. Introduction

Stenning and Plourde[1] have presented an analytical model for calculating the development of circumferential inlet distortions in multi-stage machines. The procedure they followed was to replace the stages of the compressor by an appropriate distribution of body forces. Although the analysis in the presented form assumes that all stages are identical and further requires as input an empirical resistance factor (which controls the amount of crossflow within the compressor) its simplicity makes the method valuable for initial design studies.

A more accurate survey of the perturbed flow field upstream, within and downstream of a multi-stage compressor may be obtained by using an analysis given by Dunham.[2] The mathematical model replaces rotor and stator blade rows (or, alternatively, the stages) by actuator discs. The initial assumption of small axial clearances between the blade rows has been overcome by Whitehead.[3] This latter analysis is more complex than the first.

The object of the method presented in this paper is to retain the simplicity of Stenning/Plourde's analysis but to allow all the stages to be different and to make an empirical crossflow factor unnecessary. Additionally, as numerical calculations show, the method is relatively insensitive to computational rounding errors which using the method described in (2) can dominate the solution in the case of very large axial clearances within the compressor.

II. Outline of the Theory

1. Mathematical Model

It is required to determine the pressure and velocity perturbations upstream, between the stages and downstream of a multi-stage axial compressor with a high hub-tip ratio. For this purpose an analytical model is suggested which replaces the stages of the compressor by actuator discs as shown in Fig. 1.

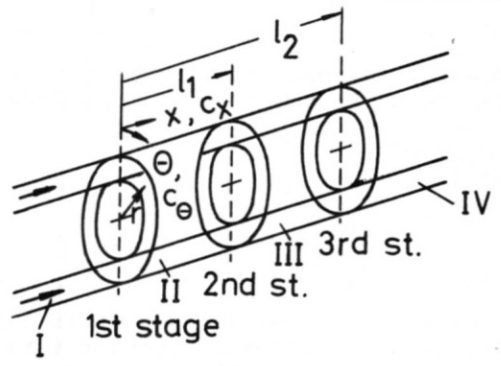

I = Flow region upstream of compressor
II = Flow region between 1st and 2nd disc
III= Flow region between 2nd and 3rd disc
IV = Flow region downstream of compressor

FIG. 1 MATHEMATICAL MODEL OF 3-STAGE COMPRESSOR

The restriction to compressors with high hub-tip ratio means that radial variations in flow properties are negligible and reduces the problem to a two-dimensional one. It may also be assumed that the flow outside the discs is steady, inviscid and incompressible.

A 3-stage compressor has been chosen as an example to demonstrate the method. The procedure is easily extended to a larger number of stages.

2. The Flow Outside the Actuator Discs

With the above assumptions and with the axial coordinate normalized using the mean compressor radius the equations of motion reduce to (†)

$$c_\theta \frac{\partial c_\theta}{\partial \theta} + c_x \frac{\partial c_\theta}{\partial x} = - \frac{1}{\rho} \frac{\partial p}{\partial \theta} \tag{1}$$

$$c_\theta \frac{\partial c_x}{\partial \theta} + c_x \frac{\partial c_x}{\partial x} = - \frac{1}{\rho} \frac{\partial p}{\partial x} \tag{2}$$

and the continuity equation becomes

$$\frac{\partial c_\theta}{\partial \theta} + \frac{\partial c_x}{\partial x} = 0 \tag{3}$$

The axial and tangential velocities and the static pressure may be separated into mean values and superimposed perturbations.

$$c_x = \bar{c}_x + c_x' \ (x,\theta) \tag{4}$$

$$c_\theta = \bar{c}_\theta + c_\theta' \ (x,\theta) \tag{5}$$

$$p = \bar{p} + p' \ (x,\theta) \tag{6}$$

Assuming the mean flow to be purely axial everywhere in the flow regions I-IV

$$\left.\begin{aligned} &\bar{c}_\theta = 0 \\ &\text{and if} \\ &c_x' \ll \bar{c}_x \\ &c_\theta' \ll \bar{c}_x \end{aligned}\right\} \tag{7}$$

substitution of equations (7) in (1), (2) and (3) gives after neglecting terms of second order in small quantities

$$\bar{c}_x \frac{\partial c_\theta'}{\partial x} = - \frac{1}{\rho} \frac{\partial p'}{\partial \theta} \tag{8}$$

$$\bar{c}_x \frac{\partial c_x'}{\partial x} = - \frac{1}{\rho} \frac{\partial p'}{\partial x} \tag{9}$$

$$\frac{\partial c_\theta'}{\partial \theta} + \frac{\partial c_x'}{\partial x} = 0 \tag{10}$$

Equations (8) and (9) may also be expressed in terms of the total pressure perturbation. Since

$$p_t = p + \frac{\rho}{2} (c_x^2 + c_\theta^2) \ , \tag{11}$$

writing

$$p_t = \bar{p}_t + p_t' \tag{12}$$

and applying equations (4), (5), (6) and (7) gives

$$p' = p_t' - \rho \bar{c}_x c_x' \tag{13}$$

again neglecting small terms.

† Nomenclature see Appendix C.

Equation (13) introduced into (8) and (9) yields:

$$\bar{c}_x \frac{\partial c_\theta'}{\partial x} - \bar{c}_x \frac{\partial c_x'}{\partial \theta} = - \frac{1}{\rho} \frac{\partial p_t'}{\partial \theta} \tag{14}$$

$$\frac{\partial p_t'}{\partial x} = 0 \tag{15}$$

Equation (15) demonstrates that the total pressure perturbation within each individual flow region is a function of θ only and hence does not change along the mean streamlines.

The inlet distortion as such may now be specified infinitely far upstream of the compressor by a given axial velocity distribution of the form

$$c_x = \bar{c}_x + \sum_{n=1}^{j} \varepsilon_n \cos n\theta \tag{16}$$

and a uniform static pressure, $p=\bar{p}$ which implies that $p' = 0$ at $x = -\infty$. Equation (16) may be abbreviated to

$$c_x = \bar{c}_x + \tilde{c}_x \tag{17}$$

It will prove useful to separate the axial velocity perturbation c_x' in equation (4) into two further parts, namely into the given far upstream axial velocity perturbation $\tilde{c}_x$ and a compressor induced velocity perturbation c_x^* whose solution has to be sought in the flow regions I to IV. Then

$$c_x^* = 0 \quad \text{at} \quad x = - \infty \tag{18}$$

since here the compressor is too far away to affect the flow. Equation (4) now becomes

$$c_x = \bar{c}_x + \tilde{c}_x(\theta) + c_x^* \ (x,\theta) \tag{19}$$

Introducing

$$c_x' = \tilde{c}_x + c_x^* \tag{20}$$

into equations (10) and (14), we have

$$\bar{c}_x \frac{\partial c_\theta'}{\partial x} - \bar{c}_x \frac{\partial c_x^*}{\partial \theta} - \bar{c}_x \frac{\partial \tilde{c}_x}{\partial \theta} = - \frac{1}{\rho} \frac{\partial p_t'}{\partial \theta} \tag{21}$$

$$\frac{\partial c_\theta'}{\partial \theta} + \frac{\partial c_x^*}{\partial x} = 0 \tag{22}$$

Differentiating equations (21) and (15) with respect to x and θ respectively and adding gives

$$\frac{\partial^2 c_x^*}{\partial \theta \partial x} - \frac{\partial^2 c_\theta'}{\partial x^2} = 0 \tag{23}$$

A solution may be attempted in the form

$$c_x^* = \sum_{n=1}^{j} S_n(x) \cos n\theta \tag{24}$$

with S_n an as yet unknown function of x. Using equ. (24) in connection with equ. (22) the tangential velocity perturbation in its general form can be determined:

$$c_\theta' = \sum_{n=1}^{j} - \frac{1}{n} \frac{dS_n(x)}{dx} \sin n\theta \qquad (25)$$

Introducing equ. (24) and equ. (25) into equ. (23) gives an ordinary differential equation for S_n.

$$\frac{d^3S_n(x)}{dx^3} - n^2 \frac{dS_n(x)}{dx} = 0 \qquad (26)$$

3. Solution in Flow Region I (Upstream)

The solution for S_n in flow region I is found from equ. (26) as

$$S_n(x) = A_n + B_n e^{-nx} + U_n e^{nx} \qquad (27)$$

where A_n, B_n, U_n are constants to be determined from the boundary conditions. As stated above, $c_x^* = 0$ at $x = -\infty$. Hence from equ. (24) it follows that A_n and B_n are zero.

Thus, with eqns. (24), (20) and (25)

$$c_x^* = \sum_{n=1}^{j} U_n e^{nx} \cos n\theta \qquad (28)$$

$$c_x' = \sum_{n=1}^{j} (\varepsilon_n + U_n e^{nx}) \cos n\theta \qquad (29)$$

$$c_\theta' = \sum_{n=1}^{j} - U_n e^{nx} \sin n\theta \qquad (30)$$

The total pressure perturbation upstream of the compressor is found from equ. (13), which may be rewritten in the following form.

$$p_t' = p' + \rho \bar{c}_x (\tilde{c}_x + c_x^*) \qquad (31)$$

At $x = -\infty$ $c_x^* = 0$ and $p' = 0$ so that equ. (31) becomes

$$p_t' = \rho \bar{c}_x \tilde{c}_x \qquad (32)$$

As mentioned above, the total pressure perturbation does not change along mean streamlines and consequently equ. (32) holds in the entire upstream flow field.

The static pressure perturbation in flow region I is found from equ. (13) with c_x' given by equ. (29).

4. Solution in Flow Region II (1st gap)

Equ. (26) is again applied in the flow region II and the solution is

$$S_n(x) = G_{n11} + G_{n12} e^{-nx} + G_{n13} e^{nx} \qquad (33)$$

where G_{n11}, G_{n12} and G_{n13} are constants to be determined from the boundary conditions described in a later chapter.

Thus with eqns. (24), (20) and (25)

$$c_x^* = \sum_{n=1}^{j} (G_{n11} + G_{n12} e^{-nx} + G_{n13} e^{nx}) \cos n\theta \qquad (34)$$

$$c_x' = \sum_{n=1}^{j} (\varepsilon_n + G_{n11} + G_{n12} e^{-nx} + G_{n13} e^{nx}) \times \cos n\theta \qquad (35)$$

$$c_\theta' = \sum_{n=1}^{j} (G_{n12} e^{-nx} - G_{n13} e^{nx}) \sin n\theta \qquad (36)$$

The difference in total pressure perturbation across a stage (see Appendix A) is found to be

$$\Delta p_t' = \rho U_b \psi' c_x' - \rho U_b c_\theta' \qquad (37)$$

In this equation ψ' is the slope of the undistorted stage characteristic at the mean flow rate under consideration (see Fig. 2).

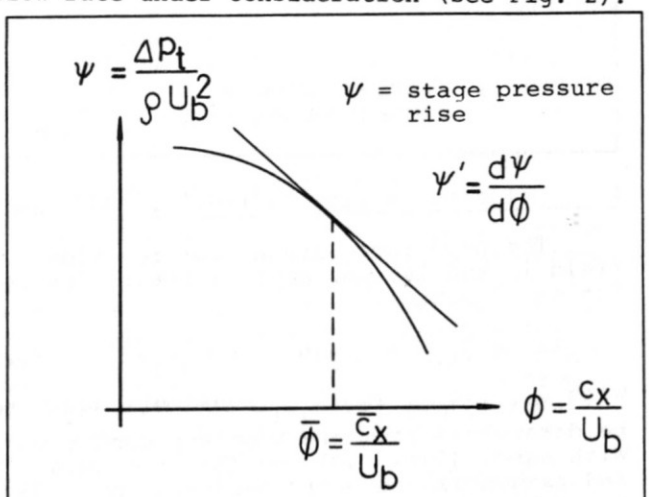

FIG. 2 SCHEMATIC DIAGRAM OF STAGE CHARACTERISTIC

c_x' and c_θ' are the axial and tangential velocity perturbations immediately upstream of the stage.

With the notation shown in Fig. 3 and ignoring the effect of the tangential velocity perturbation on the pressure rise across the disc, the total pressure perturbation downstream of the first stage (and hence in the entire first gap) is found from equ. (37).

$$(p_t')_{o+} = (p_t')_{o-} + \rho U_b \psi_o' (c_x')_{x=o} \qquad (38)$$

The total pressure perturbation immediately upstream of the stage is given by equ. (32).

$$(p_t')_{o-} = \rho \bar{c}_x \tilde{c}_x \qquad (39)$$

Introducing equ. (39) into equ. (38) yields

$$(p_t')_{o+} = \rho\bar{c}_x\tilde{c}_x + \rho U_b\psi_o'(c_x')_o \quad , \qquad (40)$$

where c_x' at x = o is found from equ. (29).

The static pressure perturbation in the first gap is then determined from the known total pressure perturbation and the axial velocity perturbation given by equ. (35)

$$p' = (p_t')_{o+} - \rho\bar{c}_x c_x' \qquad (41)$$

For $0 \leq x \leq \ell_1$

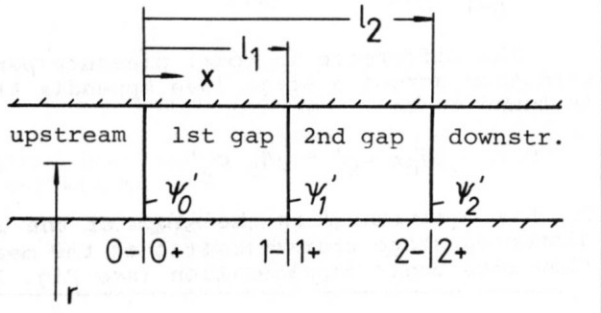

FIG. 3 CROSS-SECTION OF COMPRESSOR MODEL

5. Solution in Flow Region III (2nd gap)

The same procedure as for the flow field in the 1st gap applies here. The solution of equ. (26) is

$$S_n(x) = G_{n21} + G_{n22}e^{-nx} + G_{n23}e^{nx} \qquad (42)$$

with G_{n21}, G_{n22} and G_{n23} constants again to be determined from the boundary conditions. With eqns. (24), (20) and (25) the axial and tangential velocity perturbations are given by

$$c_x^* = \sum_{n=1}^{j} (G_{n21} + G_{n22}e^{-nx} + G_{n23}e^{nx})\cos n\theta \qquad (43)$$

$$c_x' = \sum_{n=1}^{j} (\varepsilon_n + G_{n21} + G_{n22}e^{-nx} + G_{n23}e^{nx})\cos n\theta \qquad (44)$$

$$c_\theta' = \sum_{n=1}^{j} (G_{n22}e^{-nx} - G_{n23}e^{nx}) \sin n\theta \qquad (45)$$

The total pressure perturbation downstream of the 2nd stage (and hence in the entire second gap) becomes

$$(p_t')_{1+} = (p_t')_{1-} + \rho U_b\psi_1'(c_x')_{x=\ell_1} \qquad (46)$$

Since $(p_t')_{1-} = (p_t')_{o+}$ equ. (46) with equ. (40) yields

$$(p_t')_{1+} = \rho\bar{c}_x\tilde{c}_x + \rho U_b\psi_o'(c_x')_o + \rho U_b\psi_1'(c_x')_1 \qquad (47)$$

The static pressure perturbation is found by using eqns. (13) and (44)

$$p' = (p_t')_{1+} - \rho\bar{c}_x c_x' \qquad (48)$$

For $\ell_1 \leq x \leq \ell_2$

Any further stages and gaps may be treated by the methods described above for the flow regions II and III. Although the equation for the total pressure perturbation acquires an extra term as each successive gap is encountered, an examination of eqns. (40) and (47) shows that this may be written down at once as

$$\rho U_b\psi'_{n-1}(c_x')_{n-1} \text{ for the } n^{th} \text{ gap.}$$

6. Solution in Flow Region IV (Downstream)

Solving equ. (26) for the downstream flow field gives

$$S_n(x) = D_n + N_n e^{-nx} + P_n e^{nx} \qquad (49)$$

Introducing equ. (49) into equ. (24) it is found that for $x = +\infty$ the compressor induced velocity perturbation becomes infinite. It follows that $P_n = 0$.

It is also assumed that the flow is purely axial at exit from the final stage, so that $c_\theta' = 0$ at $x = \ell_2$. Introducing

$$S_n(x) = D_n + N_n e^{-nx} \qquad (50)$$

into equ. (25) it is apparent that c_θ' can only be zero at the exit of the compressor if $N_n = 0$.

The remainder of equ. (50) introduced into equ. (24) yields

$$c_x^* = \sum_{n=1}^{j} D_n \cos n\theta \qquad (51)$$

$$c_x' = \sum_{n=1}^{j} (\varepsilon_n + D_n) \cos n\theta \qquad (52)$$

Further use of equ. (25) shows that c_θ' is not only zero at $x = \ell_2$ but in the entire downstream flow field

$$c_\theta' = 0 \text{ for } \ell_2 \leq x \leq +\infty \qquad (53)$$

From equ. (8) together with equ. (53), and from equ. (9) together with equ. (52) it follows that

$$\frac{\partial p'}{\partial \theta} = 0 \qquad (54)$$

$$\frac{\partial p'}{\partial x} = 0 \qquad (55)$$

Eqns. (54) and (55) can only be satisfied if p' = const. Assuming that p' = 0 at $x = +\infty$, it becomes clear that p' = 0 everywhere downstream of the last stage.

$$p' = 0 \text{ for } \ell_2 \leqslant x \leqslant +\infty \qquad (56)$$

The total pressure perturbation downstream of the third stage (and hence everywhere in flow region IV) is found with the help of equ. (37).

$$(p_t')_{2+} = (p_t')_{2-} + \rho U_b \psi_2' (c_x')_{x=\ell_2} \qquad (57)$$

Since $(p_t')_{2-} = (p_t')_{1+}$ equ. (57) with equ. (46) yields

$$(p_t')_{2+} = \rho \bar{c}_x \tilde{c}_x + \rho U_b \psi_o' (c_x')_o + \rho U_b \psi_1' (c_x')_1 + \rho U_b \psi_2' (c_x')_2 \qquad (58)$$

The total pressure perturbation downstream of the compressor can also be determined from equ. (13). With p' = 0 it is found that

$$(p_t')_{2+} = \rho \bar{c}_x (c_x')_2 \qquad (59)$$

where $(c_x')_2$ is given by equ. (52).

7. Boundary Conditions

Equations (29), (35), (44) and (52) show that for each harmonic number there remain 8 unknown constants to be determined.

The first boundary condition requires that the axial velocities match at each actuator disc. By using equ. (19) this leads to the following set of conditions:

$$(c_x^*)_{o-} = (c_x^*)_{o+} \qquad (60)$$

$$(c_x^*)_{1-} = (c_x^*)_{1+} \qquad (61)$$

$$(c_x^*)_{2-} = (c_x^*)_{2+} \qquad (62)$$

Introducing equ. (28) and (34) with x = 0 into equ. (60), equ. (34) and (43) with $x = \ell_1$ into equ. (61) and equ. (43) with $x = \ell_2$ together with equ. (51) into equ. (62), three equations for the determination of the unknown constants are obtained. The equations are listed in Appendix B.

The second boundary condition results from the assumption that the stator rows belonging to each stage are heavily bladed. Hence $c_\theta' = 0$ at the exit from each disc. Since for the third disc this boundary condition has been used above, two equations remain:

$$(c_\theta')_{o+} = 0 \qquad (63)$$

$$(c_\theta')_{1+} = 0 \qquad (64)$$

Introducing equ. (36) with x = 0 into equ. (63) and equ. (45) with $x = \ell_1$ into equ. (64) two further conditions for the determination of the unknown constants are obtained (see eqns. (4) and (5) in Appendix B).

The last boundary condition involves the total pressure perturbation at the exit from the last disc. By working from upstream through the various stages of the compressor, the total pressure perturbation at exit of the last disc was established by equ. (58). On the other hand the total pressure perturbation downstream of the compressor (and hence at the exit from the last disc) was also given by equ. (59). Therefore,

$$\bar{\phi}(c_x')_2 = \bar{\phi}\tilde{c}_x + \psi_o'(c_x')_o + \psi_1'(c_x')_1 + \psi_2'(c_x')_2 \qquad (65)$$

or, alternatively, by writing $c_x' = \tilde{c}_x + c_x^*$

$$\frac{\psi_o'}{\bar{\phi}}(c_x^*)_o + \frac{\psi_1'}{\bar{\phi}}(c_x^*)_1 + \left(\frac{\psi_2'}{\bar{\phi}} - 1\right)(c_x^*)_2 = -\frac{\psi_o' + \psi_1' + \psi_2'}{\bar{\phi}}\tilde{c}_x \qquad (66)$$

Introducing the appropriate expressions for the compressor induced axial velocity perturbations one further equation is obtained for the determination of the unknown constants. It is listed as equ. (8) in Appendix B.

8. Supplementary Conditions

The boundary conditions established in the previous chapter lead to the equations (60) to (65), giving 6 equations for the determination of the 8 unknown constants. Two further equations are therefore required. These are derived by observing that the solutions obtained for the velocity perturbations and total pressure perturbations in the flow regions I-IV must satisfy equations (15), (21) and (22). Eqns. (15) and (22) are immediately satisfied in all flow regions; similarly for equ. (21) upstream and downstream of the compressor. The requirement that equ. (21) is also satisfied in the 1st and 2nd gaps however leads to two further conditions for the determination of the unknown constants.

Consider first flow region II (first gap). Introducing $(c_x')_o = \tilde{c}_x + (c_x^*)_o$ into equ. (40) and taking the partial derivative with respect to θ it is found that

$$\left(\frac{\partial p_t'}{\partial \theta}\right)_{o+} = \rho \bar{c}_x \frac{\partial \tilde{c}_x}{\partial \theta} + \rho U_b \psi_o' \frac{\partial \tilde{c}_x}{\partial \theta} + \rho U_b \psi_o' \frac{\partial (c_x^*)_o}{\partial \theta} \qquad (67)$$

With this expression, equ. (21) yields

$$\frac{\psi_o'}{\bar{\phi}} \frac{\partial \tilde{c}_x}{\partial \theta} + \frac{\psi_o'}{\bar{\phi}} \frac{\partial (c_x^*)_o}{\partial \theta} + \left(\frac{\partial c_\theta'}{\partial x} - \frac{\partial c_x^*}{\partial \theta}\right) = 0 \qquad (68)$$

For $0 \leqslant x \leqslant \ell_1$

Introducing equ. (34) and (36) into the bracketed term of the last equation and integrating with respect to θ, we have

$$\frac{\psi_o'}{\bar{\phi}} \tilde{c}_x + \frac{\psi_o'}{\bar{\phi}}(c_x^*)_o - \sum_{n=1}^{j} G_{n_{11}} \cos n\theta = 0 \quad (69)$$

With the appropriate velocity perturbations introduced one further equation is obtained. This is listed in Appendix B as equ. (6).

The same procedure as above applied to the second gap produces an expression which corresponds to equ. (69).

$$\frac{\psi_o' + \psi_1'}{\bar{\phi}} \tilde{c}_x + \frac{\psi_o'}{\bar{\phi}}(c_x^*)_o + \frac{\psi_1^*}{\bar{\phi}}(c_x^*)_1 - \sum_{n=1}^{j} G_{n_{21}} \cos n\theta = 0 \quad (70)$$

Again introducing the appropriate expressions for the velocity perturbations the last equation for the determination of the unknown constants is derived (see Appendix B, equ. (7)).

9. Flow Angle Perturbations

Having determined the axial and tangential velocity perturbation at a certain axial location x the corresponding flow angle perturbation may easily be derived.

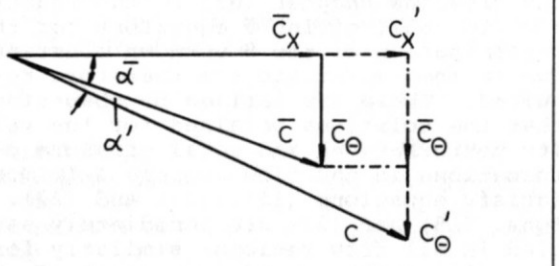

FIG. 4 VELOCITY AND FLOW ANGLE PERTURBATIONS

Assuming initially that the mean flow has an average swirl angle $\bar{\alpha}$ it follows from Fig. 4 that

$$\tan(\bar{\alpha} + \alpha') = \frac{\bar{c}_\theta + c_\theta'}{\bar{c}_x + c_x'} \quad (71)$$

Introducing

$$\bar{c}_\theta = \bar{c}_x \tan \bar{\alpha} \quad (72)$$

into equ. (71) and rearranging it is found that

$$\alpha' = \arctan\left[\frac{\bar{c}_x \tan \bar{\alpha} + c_\theta'}{\bar{c}_x + c_x'}\right] - \bar{\alpha} \quad (73)$$

From the assumption that the mean flow is purely axial everywhere in the flow regions I - IV it follows from equ. (73) with $\bar{\alpha} = 0$

$$\alpha' = \arctan \frac{c_\theta'}{\bar{c}_x + c_x'} \quad (74)$$

giving the required flow angle perturbation.

III. Comparison Between Experiment and Theory

Interstage traverse data for comparison with the analysis has been obtained from a low speed 4-stage axial flow compressor consisting of inlet guide vanes, 4 identical stages and outlet guide vanes. The compressor, which is shown schematically in Fig. 5, has a hub/tip ratio of 0.8 and a mean radius of 6.3 inches. The 50% reaction constant section blading has a circular arc camber line and stagger and camber angles of 20° and 40° respectively. The space/chord ratio at blade mid-height is 0.88 and the chord length is 0.7 inches. All gaps between the blade rows have the same width of 0.54" except that between the TE of the last stator and the LE of the OGVs which is 3.30". The distance between plane 10 and 11 is 2.0".

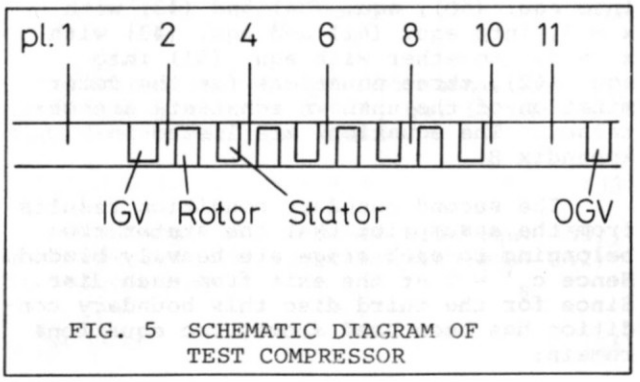

FIG. 5 SCHEMATIC DIAGRAM OF TEST COMPRESSOR

The instrumentation consists of a Kiel probe in plane 1 1.9" upstream of the LE of the IGVs, 5 cylindrical 3-hole probes behind the IGVs and each stator and a wedge probe in plane 11. All probes measure the flow at annulus mid-height.

The static pressures were obtained from outer wall tappings except in plane 11 where the pressure was taken from the wedge probe.

The flow angles were measured by balancing the instrument static pressures. No flow angles could be measured in plane 1 since only a Kiel probe had been installed. Therefore the total velocity (and not its axial component) is presented for this plane.

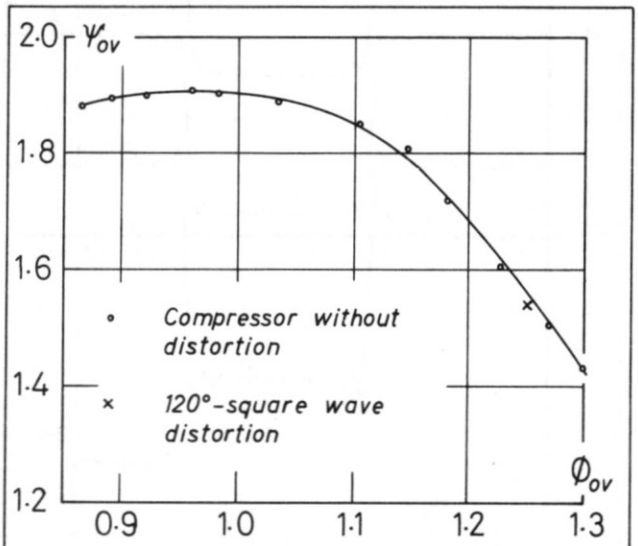

FIG. 6 OVERALL TOTAL PRESSURE RISE CHARACTERISTIC

The overall pressure rise characteristic of the undistorted compressor is shown in Fig. 6. It is based on the total pressures and an arithmetic average of the axial velocities obtained from the Kiel and wedge probes in plane 1 and 11 respectively. All tests, including that with a distorted flow were performed at a compressor speed of approximately 2980 r.p.m.

A characteristic with the flow coefficient based on measurements obtained from the calibrated airmeter together with further information concerning the compressor and its instrumentation is given in (4).

A 120°-square wave inlet distortion was generated by attaching a gauze segment to a uniform support screen located 5" or 0.8 compressor mean radii upstream of the IGVs. The relative positioning of gauze segment and instrumentation was obtained by rotating the support screen.

A mean flow coefficient was derived by averaging the perturbed velocity profiles at stations 1 and 11, and averaging in turn the values obtained at these two stations. The final value calculated was $\bar{\phi} = 1.251$. (The flow coefficient derived from airmeter measurements was 1.042). The slope of the overall characteristic at $\bar{\phi} = 1.251$ is then measured from Fig. 6 as -2.52. Assuming all four stages to be identical, the slopes of the stage characteristics are therefore $\psi' = -0.63$.

Fig. 7 shows the mathematical model representing the experimental compressor. The IGV and OGV blade rows are treated as 'stages' with zero slopes since losses in these rows are neglected (see also the top row of Table 1). The dimensions in Fig. 7 are normalised using the mean compressor radius.

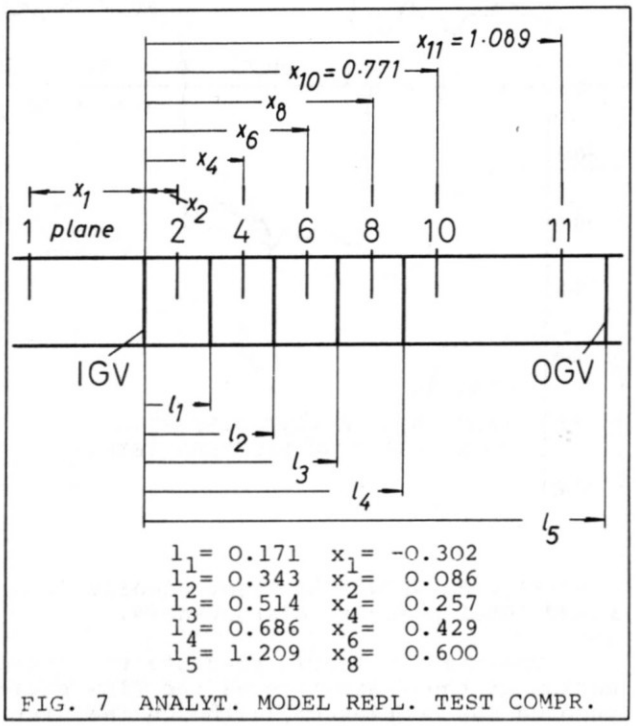

FIG. 7 ANALYT. MODEL REPL. TEST COMPR.

The experimentally obtained total pressure distortions are presented in Fig. 8a. The dashed line approximates the total pressure profile measured in plane 1 and together with the dimensions in Fig. 7, the mean flow rate and the stage slopes serves as an input to the analysis. The required relationship between the axial velocity perturbation at $x = -\infty$ and the given inlet total pressure distribution is established by equ. (32). To aid clarity in the presentation of the analytical results, the calculated total pressure perturbations are superimposed on the mean experimental pressures obtained by circumferentially averaging the appropriate curves. (The same procedure has been applied to the static pressure, flow angle and axial velocity perturbations).

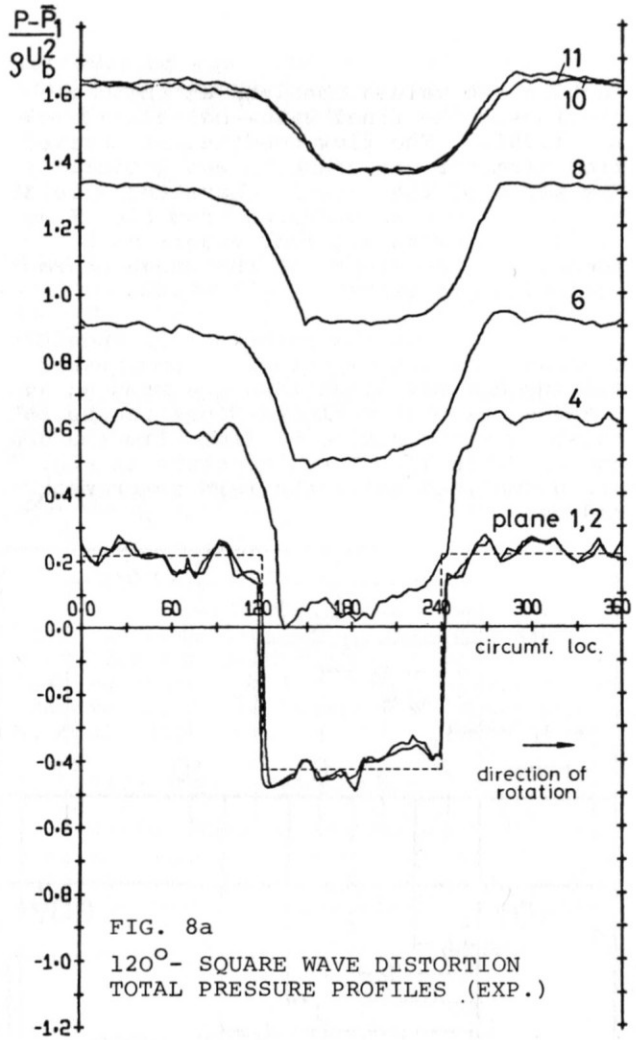

FIG. 8a
120°- SQUARE WAVE DISTORTION
TOTAL PRESSURE PROFILES (EXP.)

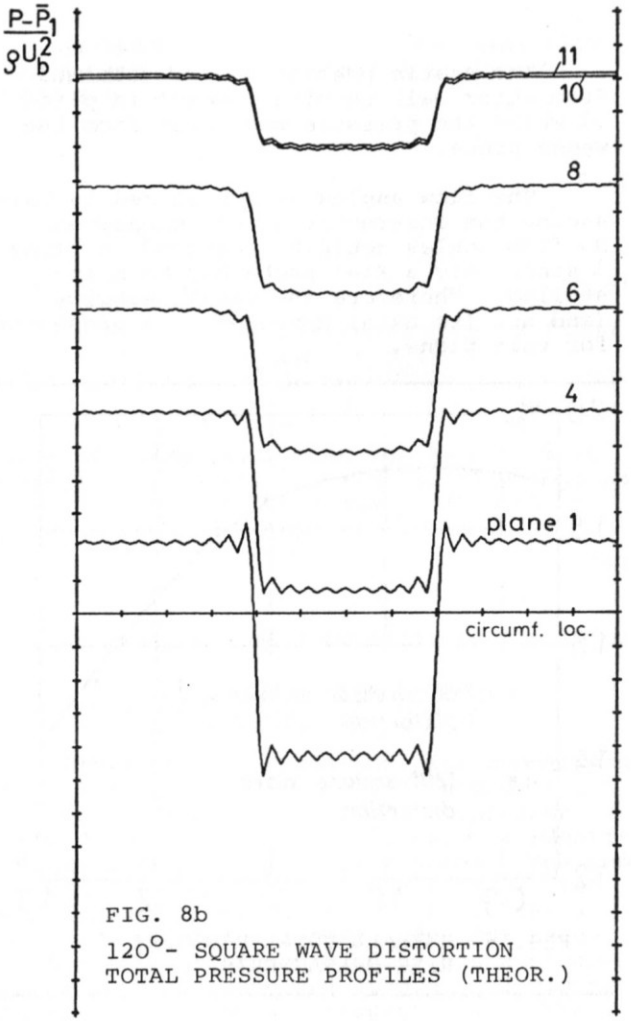

FIG. 8b
120°- SQUARE WAVE DISTORTION
TOTAL PRESSURE PROFILES (THEOR.)

Fig. 8b shows the theoretically determined total pressure disturbances.

The theory clearly predicts the attenuation of the distortion as the flow passes through the compressor, although the disturbances in plane 10 and 11 are slightly lower than demonstrated by the experiment. Difficulty in obtaining the correct slope of the stage characteristics may be responsible for this.

The experimental profiles are shifted in the direction of rotation as the flow passes from station to station. This is thought to be mainly due to the swirl of the mean flow downstream of the blade rows, contradicting the assumption of axial mean flow made in the analysis.

The theory is also unable to predict the gradual decrease in slope of the leading and trailing edge of the experimental total pressure profiles, an effect probably caused by viscosity and turbulent mixing.

The static pressure perturbations are compared in Figs. 9a, b.

The theory demonstrates the amplification of the disturbance from plane 1 to 2. The predicted uniform static pressure in planes 10 and 11 is in reasonable agreement with the experiment and a further improvement might possibly be achieved by including losses for the outlet guide vanes.

A large discrepancy arises between the theoretical and experimental profile shapes. The experimental curves show a strong asymmetry whereas the corresponding theoretical curves are symmetrical throughout. A better prediction may be obtained by the following means:

1) The inlet total pressure disturbance can be more appropriately specified by adding terms in sin nθ to equ. (16). The analysis can easily be extended to allow for these terms.

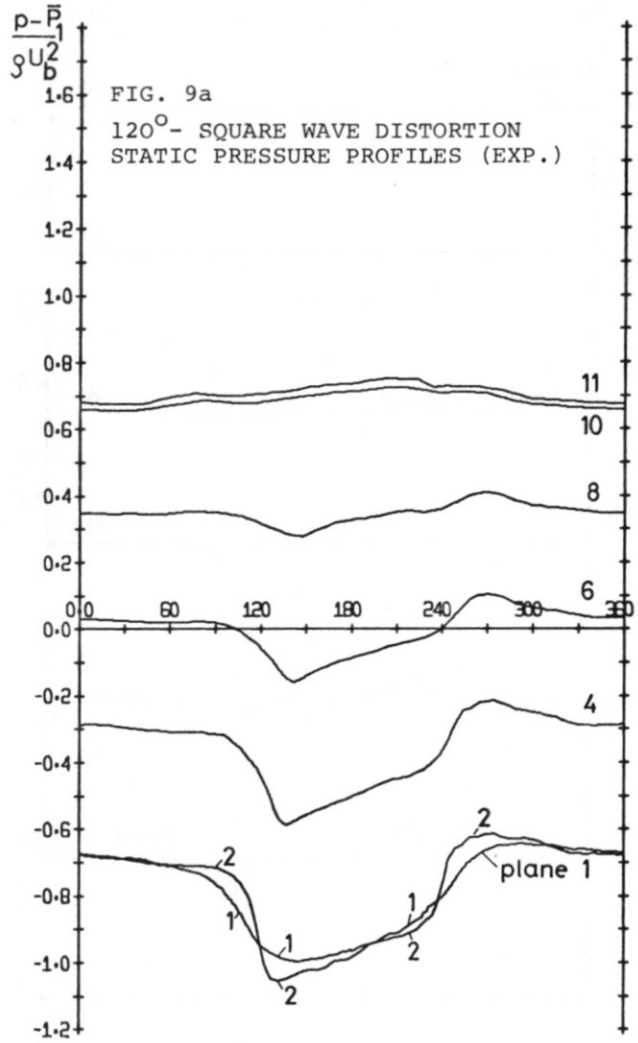

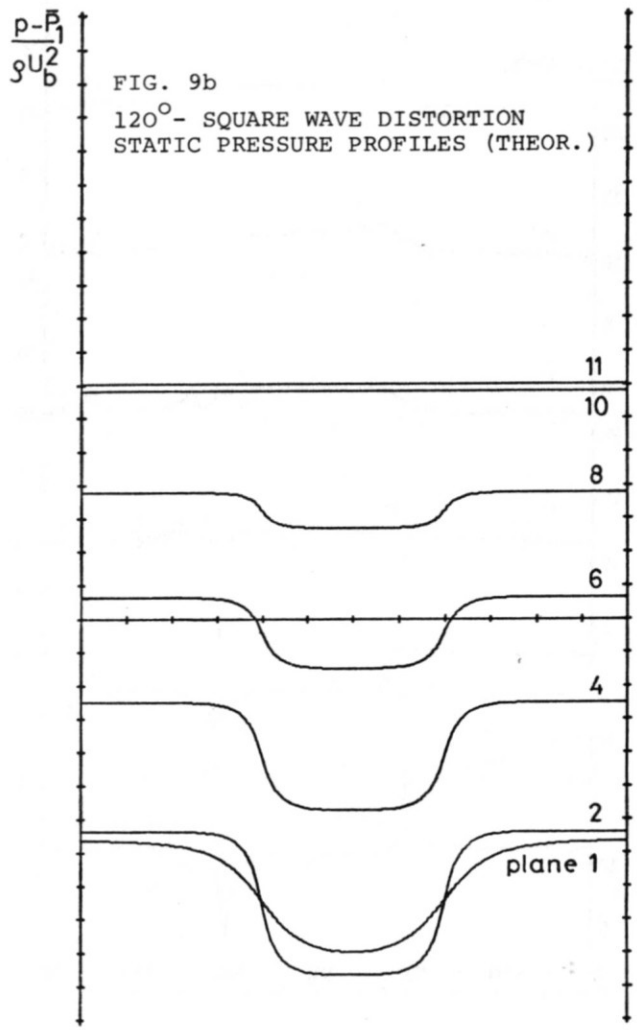

2) The effect of the tangential velocity perturbations on the pressure rise across a disc could also be accommodated in the present theory, but the number of simultaneous equations to be solved increases and the solutions lose their simplicity. The method described in (2) with the extension developed in (3) would then be preferable to the method described here.

3) All theories mentioned in this paper assume the rotor blades to respond in a quasi-steady manner to the changes in incidence which occur when the blades pass through the distorted flow. An extension to include an unsteady blade response could therefore improve the prediction.

The experimental and theoretical flow angle perturbations are presented in Figs. 10a, b. The sharp peaks in the experimental profile at 120° and 240° in plane 2 are at least partly caused by the strong total pressure gradients, which lead to a systematic error in flow angle measurements.

The axial velocity perturbations are compared in Figs. 11a, b. The agreement between the experiment and theory is good, particularly in the first three planes. In the planes further downstream the experimental curves smooth out while the theoretical ones retain their square-wave shape. It is believed (as for the total pressure profiles) that viscosity and turbulent mixing are mainly responsible. As indicated by both the experiment and theory only a little crossflow occurs within the compressor.

IV. Further Numerical Examples

1. Influence of Varying Stage Characteristics

The analysis has been used to study the effect of variable stage characteristics on the attenuation of the distortions. The compressor model used is the same as in the previous chapter and is shown in Fig. 7. If the amplitude of the first harmonic of the total pressure distortion far upstream

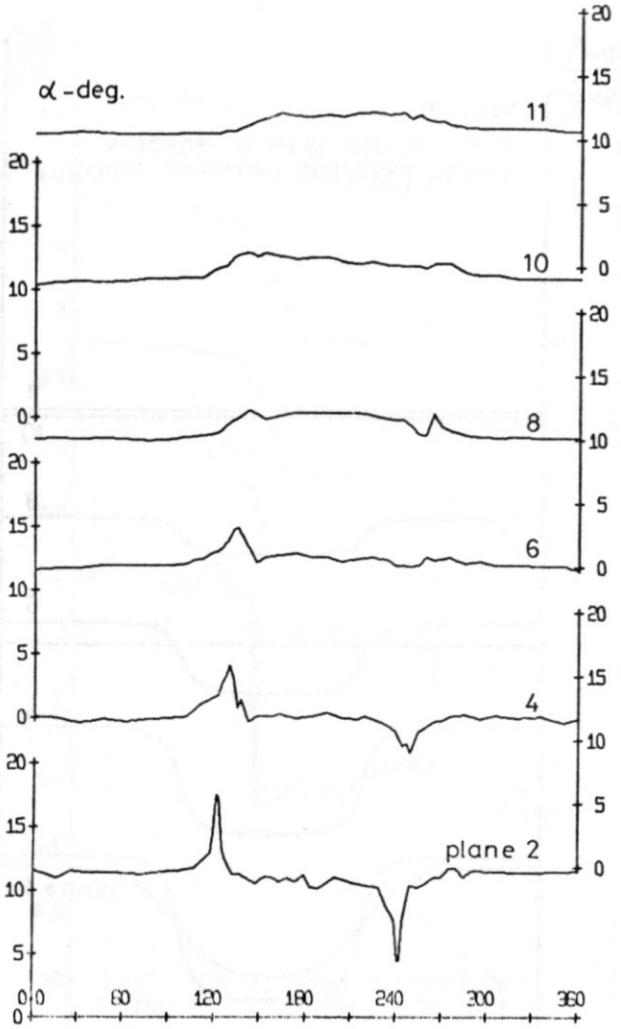

FIG. 10a
120° - SQUARE WAVE DISTORTION
FLOW ANGLES (EXP.)

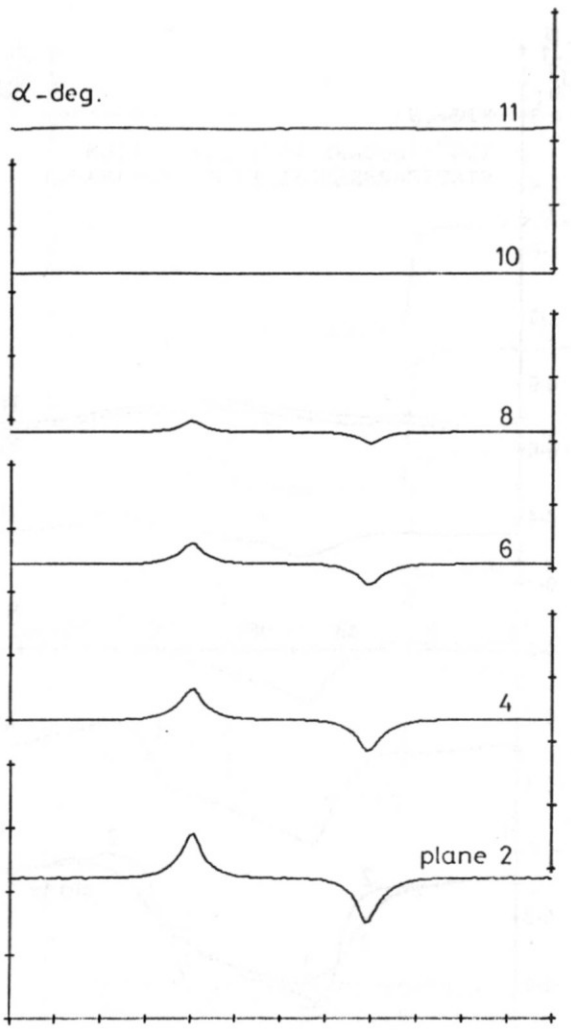

FIG. 10b
120° - SQUARE WAVE DISTORTION
FLOW ANGLES (THEOR.)

is γ and at any other axial location $|p_t'|$, then the solid line in Fig. 12 shows the ratio $\frac{|p_t'|}{\gamma}$ as a function of axial distance for slopes of the stage characteristics given by the top row in Table 1.

TABLE 1 SLOPES OF STAGE CHARACTERISTICS

Stages						
IGV	1st	2nd	3rd	4th	OGV	Σ
0	-0.63	-0.63	-0.63	-0.63	0	-2.52
0	-0.756	-0.672	-0.588	-0.504	0	-2.52
0	-0.504	-0.588	-0.672	-0.756	0	-2.52

The stages of the compressor are then rematched. The two front stages are more lightly loaded (the slope is made more negative) and the two rear stages are more heavily loaded than for the previous case. The sum of the stage slopes is the same as before. The dashed line in Fig. 12 shows that the attenuation of the total pressure distortion is higher in the front and lower in the rear stages than for the equal stage slopes. As might be expected the reverse happens when using stages with slopes given by the last row in Table 1 (see dashed-dot line in Fig. 12). The somewhat surprising result, however, is that for all three cases the amplitudes of the total pressure distortion at compressor exit are precisely the same. Real flow effects such as separation and turbulent mixing will modify this conclusion for a real machine. In [5] it is recommended that the mean loading on the earlier stages is reduced in order significantly to improve the distortion tolerance of the entire compressor.

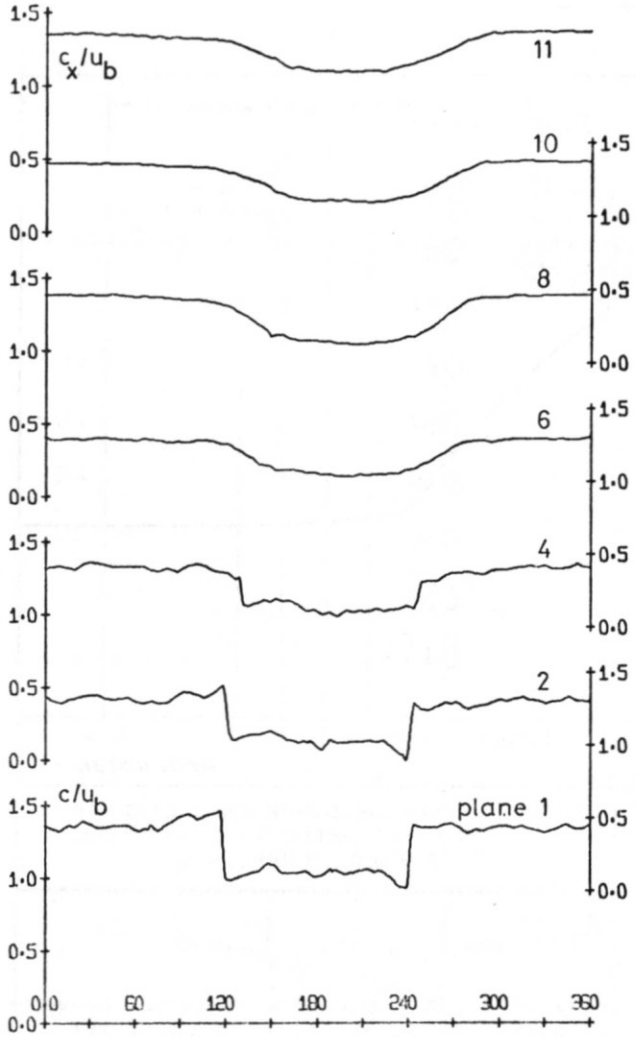

FIG. 11a
120°- SQUARE WAVE DISTORTION
AXIAL VELOCITY PROFILES (EXP.)

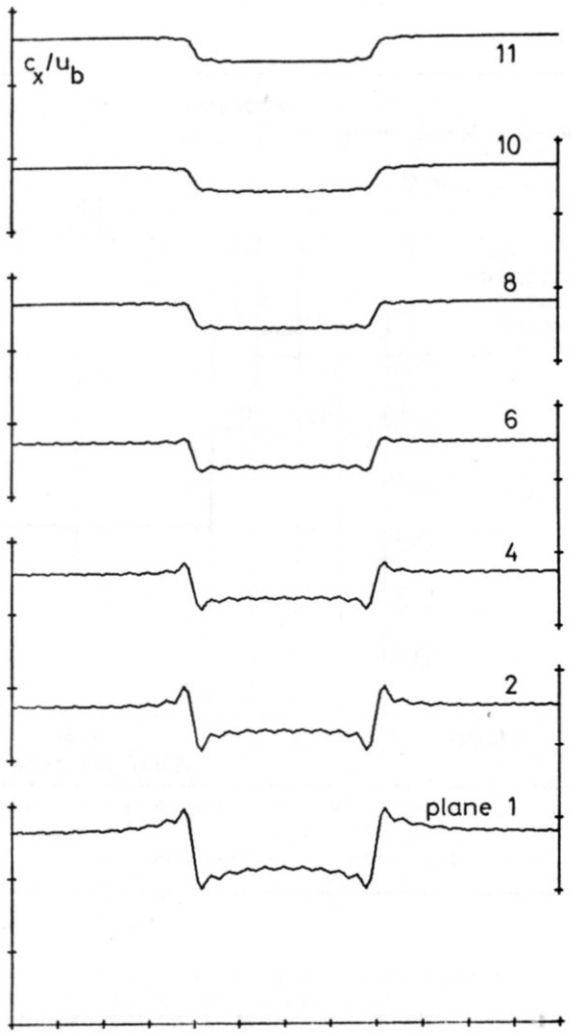

FIG. 11b
120°- SQUARE WAVE DISTORTION
AXIAL VELOCITY PROFILES (THEOR.)

The effect of varying stage characteristics on the static pressure perturbation is shown in Fig. 13. Upstream and downstream of the IGVs there is very little difference between the three patterns of stage matching. Downstream of the following stages the static pressure distortions behave in a similar manner to the total pressure disturbances.

The axial velocity perturbations are presented in Fig. 14 in the form of the ratio of the amplitude of the disturbance at any x to that at $x = -\infty$. The three ways of stage matching have so small an effect that the differences do not show in the figure.

2. Flow Redistribution in Large Axial Gap

The present analysis is used to determine the pressure and velocity perturbations upstream, within and downstream of a 2-stage compressor with a large axial clearance between the stages (see Fig. 15).

The same total pressure disturbance as given by the dashed line in Fig. 8a is assumed to exist upstream of the 2-stage compressor. The flow rate is chosen to be $\bar{\phi} = 1.251$ and the slopes of the stage characteristics to be twice those for the 4-stage compressor.

As Fig. 16 shows, the attenuation of the total pressure disturbance is considerably lower in the rear stage than in the front stage. This is due to the decay of the axial velocity distortion within the compressor as shown in Fig. 18.

The development of the static pressure perturbation as the flow approaches the compressor face is presented in the lower part of Fig. 17. There is little change from $x = -\infty$ (where the static pressure is uniform) to $x = -2.0$, but then the distortion

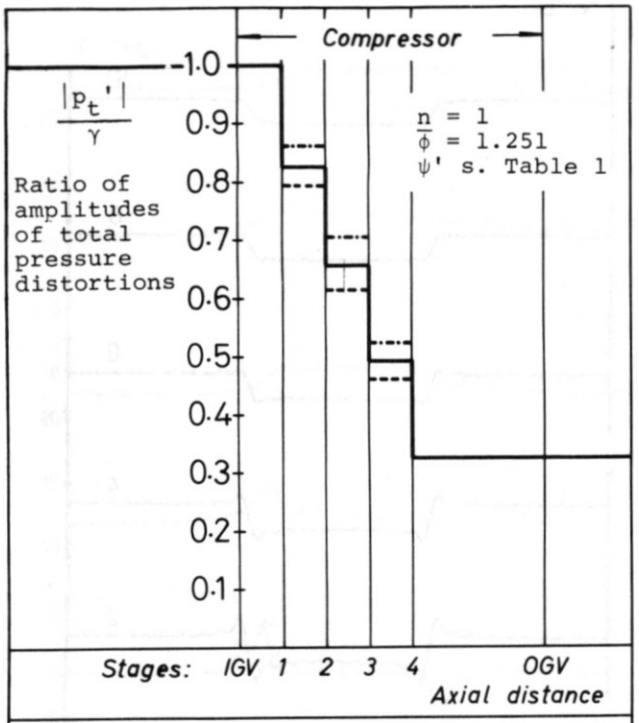

FIG. 12 EFFECT OF STAGE CHARACTERISTIC ON TOTAL PRESSURE DISTORTION IN 4-STAGE COMPRESSOR

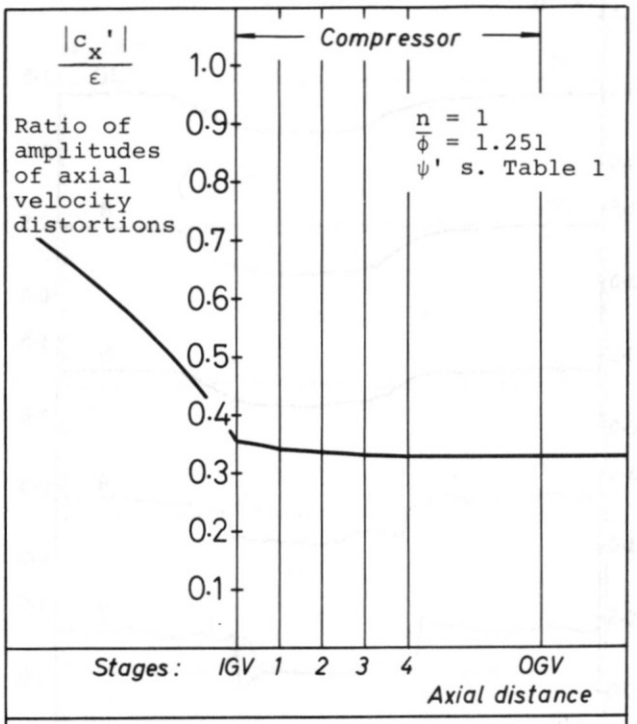

FIG. 14 EFFECT OF STAGE CHARACTERISTIC ON AXIAL VELOCITY DISTORTION IN 4-STAGE COMPRESSOR

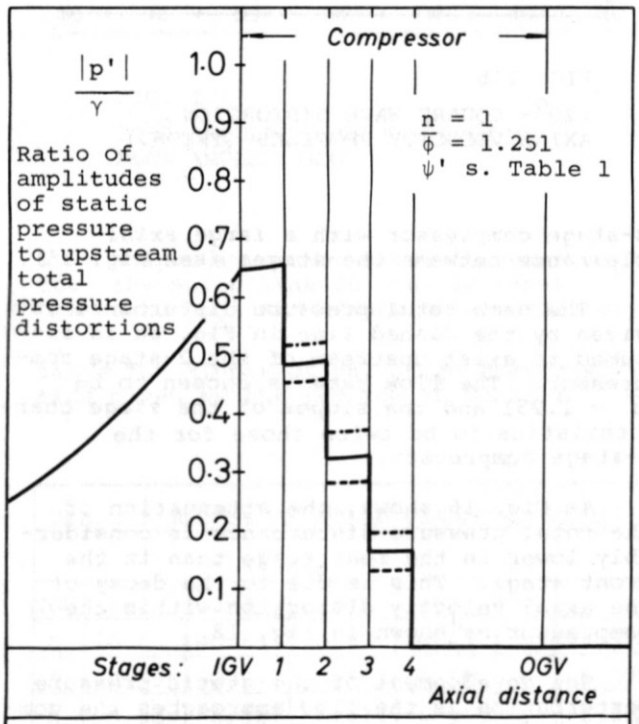

FIG. 13 EFFECT OF STAGE CHARACTERISTIC ON STATIC PRESSURE DISTORTION IN 4-STAGE COMPRESSOR

builds up at an increasing rate to the maximum perturbation at inlet to the first stage. A large attenuation takes place in the first stage itself, then in the clearance between the stages the distortion grows once more in the same way as in the upstream flow field. This is illustrated

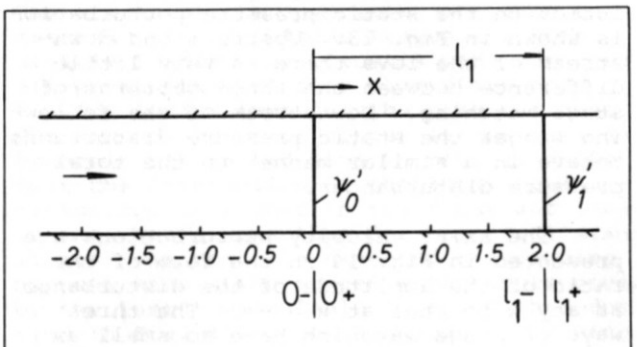

FIG. 15 ANALYTICAL MODEL REPRESENTING 2-STAGE COMPRESSOR

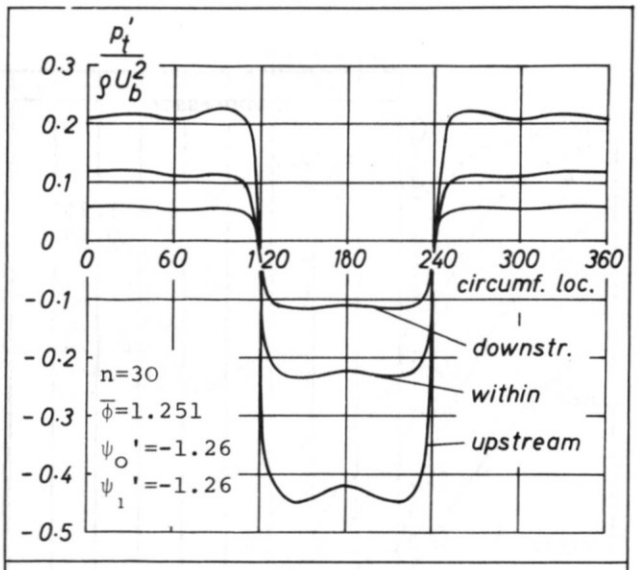

FIG. 16 TOTAL PRESSURE DISTORTION IN 2-STAGE COMPRESSOR WITH LARGE AXIAL CLEARANCE

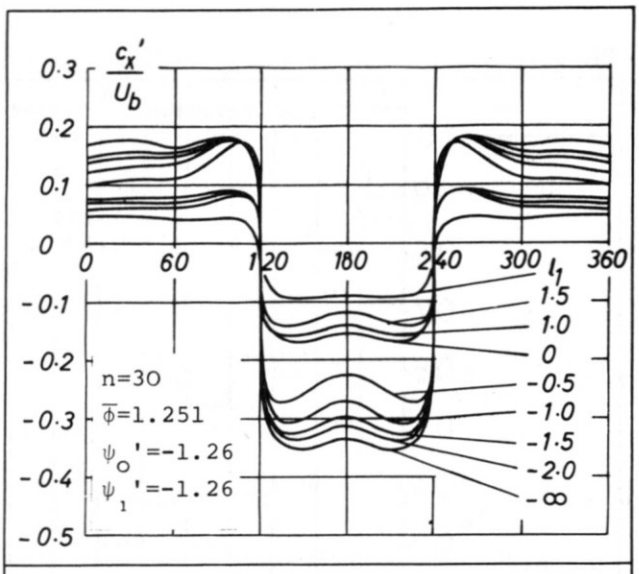

FIG. 18 AXIAL VELOCITY DISTORTION IN 2-STAGE COMPRESSOR WITH LARGE AXIAL CLEARANCE

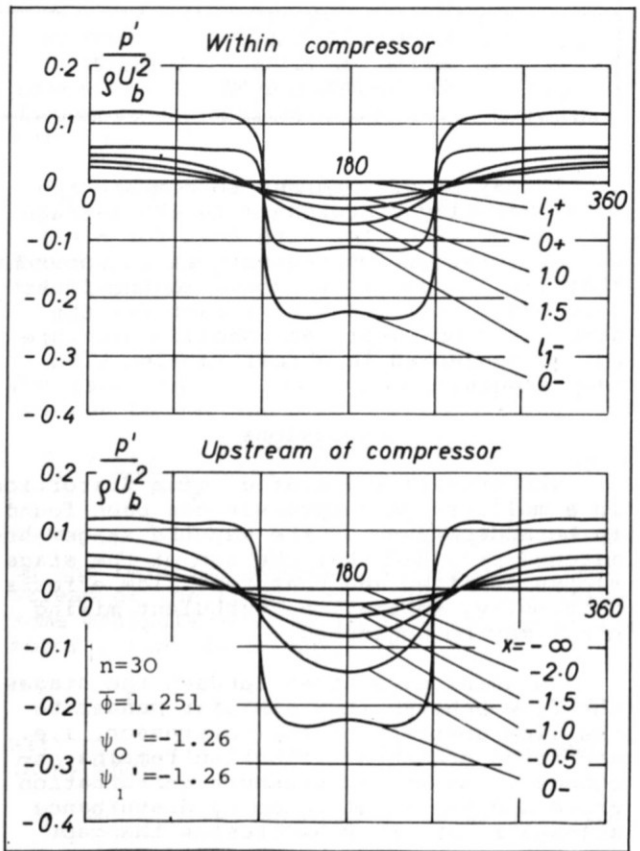

FIG. 17 STATIC PRESSURE DISTORTION IN 2-STAGE COMPRESSOR WITH LARGE AXIAL CLEARANCE

by the upper part of Fig. 17. As expected, the static pressure is uniform downstream of the second stage.

3. Inlet-distorted 10-stage Compressor

A 10-stage compressor with the same axial clearances between the stages as for the previous 4-stage compressor is subjected to the 1st, 2nd, 4th and 8th harmonic components of an inlet flow distortion. The mean flow rate is $\bar{\phi}$ = 1.251 and all stages have identical stage slopes of ψ' = - 0.63.

In Fig. 19 the total pressure perturbation ratios are presented. As illustrated, the high harmonic total pressure disturbances attenuate much more strongly in the front stages than the ones of lower order, but in the rear part of the compressor the situation is reversed. The explanation is embodied in Fig. 21. The higher order axial velocity distortions are of considerably greater magnitude at the compressor face than the lower harmonics but they then attenuate so rapidly that at the compressor exit their magnitudes are smaller than those of the lower order distortions.

The static to total pressure perturbation ratios are shown in Fig. 20. As demonstrated in Section IV.2, the static pressure disturbances grow as the flow crosses the gaps between the stages. This applies particularly to the higher harmonics.

It should be mentioned that the different behaviour of the various harmonic components within the compressor is due to the presence of axial clearances between the stages. For zero gap length all curves in Figs. 19, 20 and 21 would reduce to the same one except in the upstream flow region.

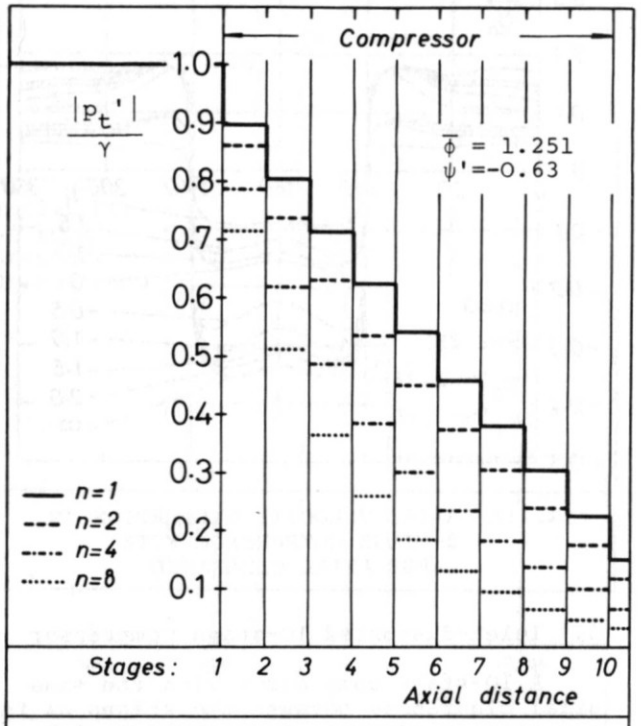

FIG. 19 EFFECT OF HARMONIC NUMBER ON TOTAL PRESSURE DISTORTION IN 10-STAGE COMPRESSOR

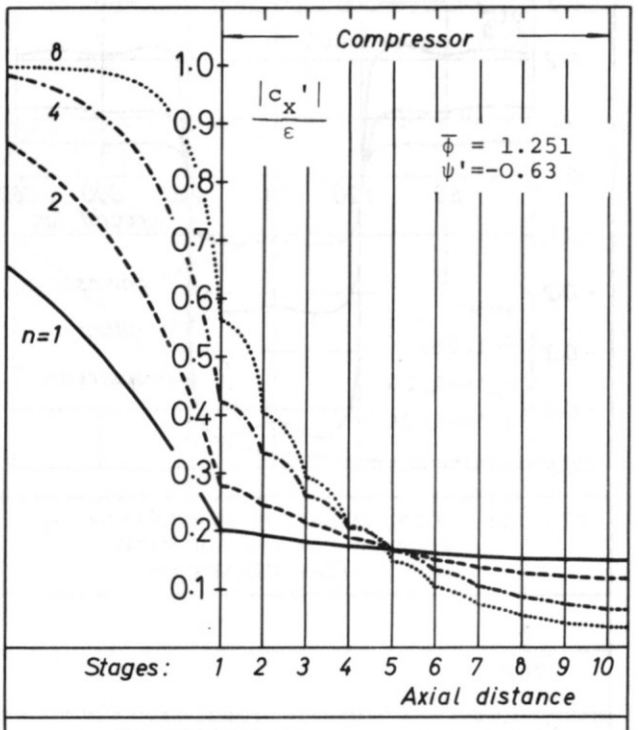

FIG. 21 EFFECT OF HARMONIC NUMBER ON AXIAL VELOCITY DISTORTION IN 10-STAGE COMPRESSOR

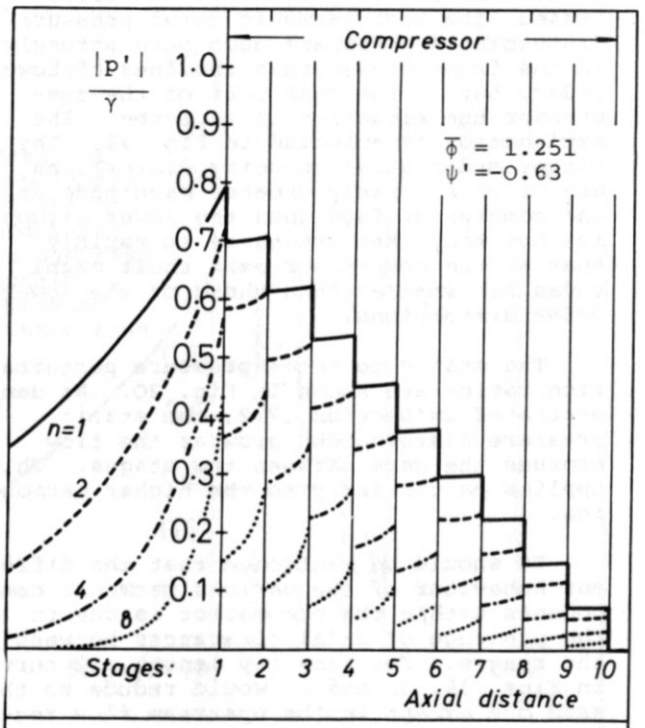

FIG. 20 EFFECT OF HARMONIC NUMBER ON STATIC PRESSURE DISTORTION IN 10-STAGE COMPRESSOR

It may be of interest to compare the axial velocity disturbance in the 4-stage compressor (Fig. 14) with that for n = 1 in the 10-stage compressor. It is apparent that little crossflow occurs in the first case but that it is significant for the 10-stage compressor, and should therefore not be neglected in a real machine with many stages.

V. Conclusions

The overall attenuation of a distortion in a multi-stage compressor has been found to be independent of the way the stages are matched provided that the sum of the stage slopes is fixed and that real flow effects (viscosity, separation, turbulent mixing etc.) may be neglected.

In axial clearances between the stages, the flow behaves in a similiar manner to the flow upstream of the compressor, i.e. the total pressure distortion remains unchanged, the static pressure perturbation grows and the axial velocity disturbance attenuates as the flow crosses the gap. This phenomenon can be observed particularly clearly for the higher harmonics of a distortion.

Both experiment and theory show that crossflow within a 4-stage compressor is small. For a 10-stage compressor, crossflow is more significant and therefore should be taken into account in an axial machine with many stages.

Appendix A

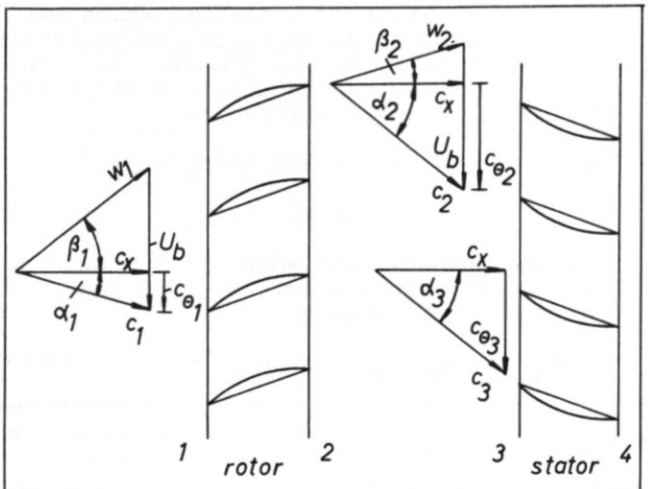

Notation

1 rotor inlet	3 stator inlet
2 rotor outlet	4 stator outlet

FIG. 22 TOTAL PRESSURE RISE ACROSS STAGE

Total Pressure Rise Across a Stage

Consider a stage as shown in Fig. 22 operating in an undistorted flow. The losses in the stator blade row can be defined as

$$\Pi_s = \frac{p_{t_3} - p_{t_4}}{\frac{1}{2}\rho c_x^2} = f(\alpha_3) \qquad (A\text{-}1)$$

The total pressure at the stator outlet then becomes

$$p_{t_4} = p_{t_3} - \frac{1}{2}\rho c_x^2 \Pi s \qquad (A\text{-}2)$$

Correspondingly, the losses in the rotor row can be defined as

$$\Pi_r = \frac{p_{t_1}^0 - p_{t_2}^0}{\frac{1}{2}\rho c_x^2} = f(\beta_1) \qquad (A\text{-}3)$$

where $p_{t_1}^0$ and $p_{t_2}^0$ are the total pressures in the relative system upstream and downstream of the rotor row. From (A-3) after some manipulation the total pressure at the rotor outlet is found:

$$p_{t_2} = p_{t_1} + \rho U_b (c_{\theta_2} - c_{\theta_1}) - \tfrac{1}{2}\rho c_x^2 \Pi_r \qquad (A\text{-}4)$$

With $p_{t_3} = p_{t_2}$ it follows from (A-2) and (A-4) that

$$p_{t_4} - p_{t_1} = \rho U_b (c_{\theta_2} - c_{\theta_1}) - \tfrac{1}{2}\rho c_x^2 (\Pi_r + \Pi_s) \qquad (A\text{-}5)$$

With $\psi = \frac{p_{t_4} - p_{t_1}}{\rho U_b^2}$ and $\phi = \frac{c_x}{u}$

equ. (A-5) becomes

$$\psi = 1 - \phi\tan\beta_2 - \phi\tan\alpha_1 - \tfrac{1}{2}\phi^2 (\Pi_r + \Pi_s) \qquad (A\text{-}6)$$

Assuming that β_2 and α_1 are independent of the flow rate ϕ, equ. (A-6) differentiated with respect to ϕ yields the slope of the stage characteristic

$$\psi' = \frac{d\psi}{d\phi} = -\tan\beta_2 - \tan\alpha_1 - \phi(\Pi_r + \Pi_s) - \tfrac{1}{2}\phi^2 \left(\frac{d\Pi_r}{d\phi} + \frac{d\Pi_s}{d\phi}\right) \qquad (A\text{-}7)$$

With the definitions

$$\Pi_r' = \frac{d\Pi_r}{d(\tan\beta_2)} \text{ and } \Pi_s' = \frac{d\Pi_s}{d(\tan\alpha_3)} \qquad (A\text{-}8)$$

it may be shown that

$$\frac{d\Pi_r}{d\phi} = -\Pi_r' \frac{1}{\phi^2} \text{ and } \frac{d\Pi_s}{d\phi} = -\Pi_s' \frac{1}{\phi^2} \qquad (A\text{-}9)$$

Equations (A-9) introduced into (A-7) yield

$$\psi' = \tfrac{1}{2}(\Pi_r' + \Pi_s') - \phi(\Pi_r + \Pi_s) - \tan\alpha_1 - \tan\beta_2 \qquad (A\text{-}10)$$

Equ. (A-10), which was also derived by Dunham [2] in a somewhat different way, establishes the connection between the stage and blade row characteristics.

Now consider the stage to operate with a circumferentially distorted flow. Using equ. A-5 the difference in total pressure across the stage is given by

$$p_{t_4} - p_{t_1} = \rho U_b (U_b - c_x\tan\beta_2 - c_{\theta_1}) - \tfrac{1}{2}\rho c_x^2 (\Pi_r + \Pi_s) \qquad (A\text{-}11)$$

where all flow properties (apart from ρ and U_b) are functions of the circumferential location Θ. It may, however, be assumed that the rotor is heavily bladed so that β_2 does not vary with Θ.

By taking the total differential of equ. (A-11) the difference of the total pressure perturbation across the stage (as a function of the axial and tangential velocity perturbation immediately upstream of the stage) is derived.

$$\delta p_{t_4} - \delta p_{t_1} = \rho U_b (-\tan\beta_2 \delta c_x - \delta c_{\theta_1}) - \rho \bar{c}_x \delta c_x (\Pi_r + \Pi_s) - \tfrac{1}{2}\rho \bar{c}_x^2 (\delta\Pi_r + \delta\Pi_s) \qquad (A\text{-}12)$$

$\delta\Pi_s$ may now be expressed as

$$\delta\Pi_s = \frac{\delta\Pi s}{\delta(\tan\alpha_3)} \delta(\tan\alpha_3) = \Pi_s' \delta(\tan\alpha_3) \qquad (A\text{-}13)$$

With

$$\tan\alpha_3 = \tan\alpha_2 = \frac{U_b}{c_x} - \tan\beta_2 \qquad (A\text{-}14)$$

which includes the assumption that the rotor is followed closely by the stator, equ. (A-13) becomes

$$\delta\Pi_s = -\Pi_s' \frac{U_b}{\bar{c}_x^2} \delta c_x \qquad (A\text{-}15)$$

A similar expression is derived for $\delta\Pi_r$.

$$\delta\Pi_r = \Pi_r' \frac{1}{\bar{c}_x}(-U_b\delta c_x - \bar{c}_x\delta c_{\theta_1} + \tan\bar{\alpha}_1\bar{c}_x\delta c_x) \qquad \text{(A-16)}$$

Substituting eqns. (A-15) and (A-16) into equ. (A-12) (and writing δc_x as c_x' etc.) it is found that

$$\Delta p_t' = \rho U_b c_x'\{\tfrac{1}{2}(\Pi_r' + \Pi_s') - \bar{\phi}(\Pi_r + \Pi_s) - \tan\bar{\alpha}_1 - \tan\beta_2\} + \rho U_b \tan\bar{\alpha}_1 c_x'(1 - \tfrac{1}{2}\bar{\phi}\Pi_r') - \rho U_b c_{\theta_1}' \times (1 - \tfrac{1}{2}\bar{\phi}\Pi_r') \qquad \text{(A-17)}$$

Assuming now that equ. (A-10), which was derived for a stage operating in undistorted flow, also holds for the mean flow in the case of a circumferential distortion, equ. (A-17) can be written as

$$\Delta p_t' = \rho U_b\{\psi' + \tan\bar{\alpha}_1(1 - \tfrac{1}{2}\bar{\phi}\Pi_r')\}c_x' - \rho U_b \times (1 - \tfrac{1}{2}\bar{\phi}\Pi_r')c_{\theta_1}' \qquad \text{(A-18)}$$

For the special case when $\Pi_r' = 0$ and the mean flow is purely axial, i.e. $\tan\bar{\alpha}_1 = 0$, equ. (A-18) reduces to

$$\Delta p_t' = \rho U_b \psi' c_x' - \rho U_b c_{\theta_1}' \qquad \text{(A-19)}$$

Appendix B

The boundary conditions and supplementary conditions lead to 8 simultaneous linear equations for the determination of the 8 unknown constants. The equations are listed below.

Upstr.	*1st Gap*			*2nd Gap*			*Downstr.*			
$\frac{U_n}{\epsilon_n}$	$-\frac{G_{n11}}{\epsilon_n}$	$-\frac{G_{n12}}{\epsilon_n}$	$-\frac{G_{n13}}{\epsilon_n}$					$=$	0	(B-1)
	$\frac{G_{n11}}{\epsilon_n}$	$+e^{-n\ell_1}\frac{G_{n12}}{\epsilon_n}$	$+e^{n\ell_1}\frac{G_{n13}}{\epsilon_n}$	$-\frac{G_{n21}}{\epsilon_n}$	$-e^{-n\ell_1}\frac{G_{n22}}{\epsilon_n}$	$-e^{n\ell_1}\frac{G_{n23}}{\epsilon_n}$		$=$	0	(B-2)
				$\frac{G_{n21}}{\epsilon_n}$	$+e^{-n\ell_2}\frac{G_{n22}}{\epsilon_n}$	$+e^{n\ell_2}\frac{G_{n23}}{\epsilon_n}$	$-\frac{D_n}{\epsilon_n}$	$=$	0	(B-3)
		$\frac{G_{n12}}{\epsilon_n}$	$-\frac{G_{n13}}{\epsilon_n}$					$=$	0	(B-4)
					$e^{-n\ell_1}\frac{G_{n22}}{\epsilon_n}$	$-e^{n\ell_1}\frac{G_{n23}}{\epsilon_n}$		$=$	0	(B-5)
$\frac{\psi_0'}{\bar{\phi}}\frac{U_n}{\epsilon_n}$	$-\frac{G_{n11}}{\epsilon_n}$							$=$	$-\frac{\psi_0'}{\bar{\phi}}$	(B-6)
$\frac{\psi_0'}{\bar{\phi}}\frac{U_n}{\epsilon_n}$	$+\frac{\psi_1'}{\bar{\phi}}\frac{G_{n11}}{\epsilon_n}$	$+\frac{\psi_1'}{\bar{\phi}}e^{-n\ell_1}\frac{G_{n12}}{\epsilon_n}$	$+\frac{\psi_1'}{\bar{\phi}}e^{n\ell_1}\frac{G_{n13}}{\epsilon_n}$	$-\frac{G_{n21}}{\epsilon_n}$				$=$	$-\frac{\psi_0'+\psi_1'}{\bar{\phi}}$	(B-7)
$\frac{\psi_0'}{\bar{\phi}}\frac{U_n}{\epsilon_n}$	$+\frac{\psi_1'}{\bar{\phi}}\frac{G_{n11}}{\epsilon_n}$	$+\frac{\psi_1'}{\bar{\phi}}e^{-n\ell_1}\frac{G_{n12}}{\epsilon_n}$	$+\frac{\psi_1'}{\bar{\phi}}e^{n\ell_1}\frac{G_{n13}}{\epsilon_n}$				$+\left(\frac{\psi_2'}{\bar{\phi}}-1\right)\frac{D_n}{\epsilon_n}$	$=$	$-\frac{\psi_0'+\psi_1'+\psi_2'}{\bar{\phi}}$	(B-8)

Appendix C

Nomenclature

c	velocity
ℓ	distance from compressor face to a disc replacing a stage
n	number of harmonic
p	static pressure
P	total pressure, identical with p_t
r	compressor mean radius
U_b	blade speed
x	axial distance normalised using the compressor mean radius
α	absolute flow angle
β	relative flow angle
γ	amplitude of upstream total pressure distortion
δ	total differential
Δ	difference between inlet and outlet of stage or compressor

ε amplitude of far upstream axial velocity distortion
Θ angle in circumferential direction
Π_s loss coefficient for stator, equ. (A-1)
Π_r loss coefficient for rotor, equ. (A-3)
ρ density
ϕ flow coefficient
ψ' slope of undistorted stage characteristic

Subscripts

n number of harmonic
r rotor
s stator
t total
x axial
ov overall
θ tangential

Superscripts

' perturbation
* compressor induced
$\sim$ far upstream perturbation
^{0} in the relative system
- average

References

1. Stenning, A.H. and Plourde, G.A. "The Attenuation of Circumferential Inlet Distortion in Multi-stage Axial Compressors", AIAA Paper No. 67-415, 1967.

2. Dunham, J. "Non-axisymmetric Flows in Axial Compressors", Ph.D. thesis, 1962, Cambridge University, Eng. Dept.

3. Whitehead, D.S. "The Decay of Inlet Disturbances in the Q.E.2 H.P. Turbine", Unpublished report, 1969, Cambridge University, Eng. Dept.

4. Mokelke, H. "The Unsteady Response of an Axial Flow Compressor with a Distorted Inlet Flow", A.R.C. C.P. 1203, 1972.

5. Langston, C.E. "Distortion Tolerance - By Design Instead of by Accident", A.S.M.E. 69-GT-115, 1969.

Acknowledgements

The test compressor referred to belongs to the Derby and District College of Technology, Derby, England and the author is grateful to the college for permission to use it for his experiments. He also wishes to thank Professor J. H. Horlock and Dr. J. P. Gostelow for their help and encouragement during the progress of the work.